Structure of the *Escherichia coli* Antitoxin MqsA (YgiT/b3021) Bound to Its Gene Promoter Reveals Extensive Domain Rearrangements and the Specificity of Transcriptional Regulation*[S]

Breann L. Brown[‡], **Thomas K. Wood**[§], **Wolfgang Peti**[‡], **and Rebecca Page**[¶1]

From the ‡Department of Molecular Pharmacology, Physiology, and Biotechnology and the ¶Department of Molecular Biology, Cell Biology, and Biochemistry, Brown University, Providence, Rhode Island 02912 and the §Artie McFerrin Department of Chemical Engineering, Texas A & M University, College Station, Texas 77843

Bacterial cultures, especially biofilms, produce a small number of persister cells, a genetically identical subpopulation of wild type cells that are metabolically dormant, exhibit multidrug tolerance, and are highly enriched in bacterial toxins. The gene most highly up-regulated in *Escherichia coli* persisters is *mqsR*, a ribonuclease toxin that, along with *mqsA*, forms a novel toxin·antitoxin (TA) system. Like all known TA systems, both the MqsR·MqsA complex and MqsA alone regulate their own transcription. Despite the importance of TA systems in persistence and biofilms, very little is known about how TA modules, and antitoxins in particular, bind and recognize DNA at a molecular level. Here, we report the crystal structure of MqsA bound to a 26-bp fragment from the *mqsRA* promoter. We show that MqsA binds DNA predominantly via its C-terminal helix-turn-helix domain, with direct binding of recognition helix residues Asn[97] and Arg[101] to the DNA major groove. Unexpectedly, the structure also revealed that the MqsA N-terminal domain interacts with the DNA phosphate backbone. This results in a more than 105° rotation of the N-terminal domains between the free and complexed states, an unprecedented rearrangement for an antitoxin. The structure also shows that MqsA bends the DNA by more than 55° in order to achieve symmetrical binding. Finally, using a combination of biochemical and NMR studies, we show that the DNA sequence specificity of MqsA is mediated by direct readout.

Biofilms, complex communities of bacteria that are encased in an extracellular matrix and adhere to almost any surface, are responsible for more than 65–80% of human infections (1,

2). Moreover, these infections are extremely difficult to treat because biofilms are both highly resistant to host defenses and tolerant to antimicrobials (3). Currently, a detailed understanding of how biofilms assemble, how they are regulated at a molecular level, and how they achieve antibiotic resistance is only rudimentarily understood. One significant mechanism by which biofilms achieve antibiotic tolerance is through the formation of bacterial persister cells (4–6). Persisters are phenotypic variants of the bulk culture that are slow growing and non-dividing (7). They are also exceptionally tolerant to antibiotics and able to survive (or "persist") exposure to antibiotic concentrations that are toxic for regular cells (4, 7, 8). Although the frequency of persisters is only about 1 in 1 million in planktonic cultures (9), the frequency is as high as 1 in 100 in biofilms (10). The increased incidence of persister cells in biofilms and their role in human bacterial infections have stimulated renewed efforts to understand the molecular mechanism(s) that underlies the persister phenotype.

Recent studies have demonstrated that the frequency at which persisters occur in populations of *Escherichia coli* is determined by the expression of chromosomal toxin·antitoxin (TA)[2] genes (4, 8, 11, 12). TA pairs are composed of two genes organized in an operon that encode an unstable, labile antitoxin and a stable toxin, which associate to form a stable complex (13–17). There are currently nine established toxin families (18), and similarities between toxins in fold and function are slowly emerging (19, 20). However, there is much greater diversity in structure and toxin recognition among antitoxins. TA systems are regulated by distinct differences in their lifetimes (21). Thus, the most important hallmark of antitoxins is their ability to be rapidly degraded by proteolysis. Under silent conditions, the activity of the toxin is blocked by the antitoxin. However, under conditions of stress, the antitoxins are degraded by proteases (21–24). This degradation outpaces the formation of the TA complex and leads to rapid growth arrest by the cellular effects of the toxin (25–27). TA complexes also regulate their own transcription, where the antitoxins bind to the promoter DNAs within their own operons and the cognate toxins enhance DNA binding (28–31). Although it is

[2] The abbreviations used are: TA, toxin·antitoxin; HTH, helix-turn-helix; MqsA-F, full-length MqsA; MqsA-N, N-terminal toxin-binding domain of MqsA; MqsA-C, C-terminal XRE-HTH domain of MqsA.

believed that multiple factors play important roles in TA expression, stability, and transcription regulation, a detailed molecular picture of the structural transitions that are required for DNA binding and recognition by TA pairs, and antitoxins in particular, is largely missing.

The gene most highly up-regulated in *E. coli* persister cells is *mqsR* (motility quorum-sensing regulator, *ygiU*/*b3022*) (12, 32, 33). Recently, we determined the crystal structures of MqsA alone and the MqsR·MqsA complex and showed that the *mqsRA* operon defines a novel family of TA systems in *E. coli*, in which MqsR is the toxin and MqsA is the antitoxin (19). The structure revealed that the MqsR toxin is a ribonuclease belonging to the RelE bacterial toxin family (19, 34, 35). MqsR is unique because it is the first toxin linked to biofilms and quorum sensing (33) and is the first toxin that, when deleted, decreases persister cell formation (31). The antitoxin MqsA is even more unusual because it is the first antitoxin that requires a metal, zinc, for structural stability (19); it is the only *E. coli* antitoxin that is structured throughout its entire sequence; and it is the first antitoxin demonstrated to bind DNA via its C-terminal and not N-terminal domain (19, 27, 36–39). Critically, in addition to binding its own promoter (19, 34, 35, 40), MqsA and the MqsR·MqsA complex are also the only known antitoxin/TA pair that bind not only their own promoter but also the promoters of other genes that play important roles in *E. coli* physiology, including *mcbR* and *spy* (19) as well as *cspD* (31). Moreover, although 14 antitoxin structures have been solved to date, their primary sequences are highly divergent when compared with MqsA (supplemental Table S1) because the sequence identity between MqsA and the most closely related antitoxin, the *E. coli* protein HigA, is only 13%.

We recently showed that MqsA is a dimer, with the MqsR·MqsA complex forming a heterotetramer of composition MqsR·MqsA$_2$·MqsR. MqsA is composed of an N-terminal zinc-binding domain, MqsA-N, which binds MqsR, and a C-terminal helix-turn-helix (HTH) domain, MqsA-C, which binds DNA and mediates dimerization (19). Electrophoretic mobility shift assays (EMSAs) showed that DNA binding is mediated exclusively by MqsA-C because MqsA-N both alone and in complex with MqsR is not capable of binding the *mqsRA* promoter (P*mqsRA*) (19). However, the atomic resolution structure of MqsA suggested that the MqsA-N domains may also play a role in DNA binding. In addition, EMSA studies showed that the MqsR·MqsA complex binds P*mqsRA* DNA with a higher affinity than MqsA alone (35), suggesting that MqsR may also interact with DNA. Finally, the palindromic sequence of P*mqsRA* is separated by a TA tract, which typically leads to changes in DNA curvature (41). This suggests that MqsA recognition of P*mqsRA* DNA may be achieved using a combination of both direct readout (direct discriminatory contacts are made between the protein and the bases in the major groove) and indirect readout (no direct contacts are made between the protein and the bases, and, instead, specificity is achieved by water-mediated hydrogen bonding and/or the induction of DNA distortion) (42, 43).

In order to understand the structural basis of DNA binding, regulation, and specificity by the MqsA antitoxin, the x-ray

crystallographic structure of MqsA bound to a 26-base pair DNA fragment derived from the *mqsRA* promoter was determined. These studies reveal that MqsA undergoes extensive domain rearrangements upon DNA binding and explains why both full-length MqsA and the MqsR·MqsA complex bind DNA with higher affinities than MqsA-C alone. A combination of EMSA competition assays and NMR spectroscopy titration studies was then used to show that MqsA recognizes P*mqsRA* DNA using direct readout, which is mediated by MqsA residues Asn[97] and Arg[101]. Finally, our studies reveal that the MqsR·MqsA complex probably uses a mechanism of co-transcriptional regulation in which both MqsA and MqsR bind directly to DNA and provides further evidence that MqsA utilizes steric occlusion to mitigate MqsR-mediated toxicity.

EXPERIMENTAL PROCEDURES

Expression, Purification, and Crystallization—Full-length MqsA (residues 1–131; MqsA-F), MqsA N-terminal domain (residues 1–76; MqsA-N), and MqsA C-terminal domain (residues 62–131; MqsA-C) were cloned and expressed as described previously (19). Multiple DNA duplexes that correspond to the palindromic region of P*mqsRA* were prepared and screened for crystallization with MqsA as described previously (44). Briefly, the MqsA P*mqsRA* dsDNA complex that formed crystals suitable for structure determination (hereafter referred to as MqsA·P*mqsRA*) was prepared by incubating 24 μM MqsA with 30 μM P*mqsR*A dsDNA (TGTAAT<u>TAAC-CT</u>TTT<u>AGGTTA</u>TAACT; palindrome is underlined) in protein stabilization buffer (10 mM Tris, pH 7.0, 50 mM NaCl, 0.5 mM Tris(2-carboxyethyl)phosphine hydrochloride). After incubation at room temperature for 30 min, the complex was concentrated 10-fold using a 3000 Da molecular mass cutoff centrifugal filter (Millipore) and immediately subjected to crystallization trials. A single merohedrally twinned crystal of the MqsA·P*mqsRA* complex formed in 0.2 M ammonium chloride, 20% PEG 3350 at 4 °C in a drop containing 0.2 μl of protein and 0.4 μl of crystallization condition.

Data Collection and Structure Determination—The MqsA·P*mqsRA* crystal was cryoprotected by a short soak in mother liquor supplemented with 20% glycerol and then frozen by direct transfer to liquid nitrogen. This crystal diffracted to 2.1 Å. X-ray diffraction data were collected at the NSLS X25 microfocus beamline at a wavelength of 0.9788 Å using an ADSC Q315 CCD detector. Data were indexed, integrated, and scaled with *DENZO* and *SCALEPACK* from the *HKL-2000* program package (45). As reported previously (44), analysis with *phenix.xtriage* (46) confirmed the space group of P4$_1$ or P4$_3$ with a twin fraction of 0.372 and twin operator h,-k,-l. Phase determination and structure solution were performed with two successive rounds of molecular replacement using Phaser (47). First, a search was performed with two copies of the MqsA N-terminal domain (PDB entry 3GA8) and two copies of the MqsA C-terminal domain (PDB entry 3FMY). This produced a single solution in P4$_1$. A second round of molecular replacement was then used to search for an additional four copies of a 5-mer DNA duplex. A single solution was obtained with a final log likelihood gain of 975.

The R_{free} set (9.42%) was assigned using Phenix with the appropriate twin operator. Subsequent model building was performed in Coot (48), and model refinement was performed with Phenix (46) using NCS. The model contains one complex (one MqsA dimer complexed with one DNA duplex) with a total of 264 protein residues and 52 nucleotides. The electron density of the bound DNA is shown in supplemental Fig. S1. Analysis of DNA parameters was carried out using the programs Curves+ (49), 3DNA (50), and Entanlge (51).

Mutagenesis—Amino acid mutagenesis was carried out using the QuikChange mutagenesis kit (Stratagene), and all constructs were sequenced (Agencourt). Mutated DNA constructs were purchased as individual complementary oligonucleotides (Integrated DNA Technologies) and then annealed as described previously (44).

NMR Analysis—For all NMR studies, the C-terminal domain of MqsA (MqsA-C) was expressed in M9 minimal medium containing selective antibiotics and 4 g/liter D-[^{13}C]glucose and/or 1 g/liter ^{15}NH$_4$Cl (Cambridge Isotope Laboratories, Cambridge, MA) as the sole carbon and nitrogen sources, respectively.

Purification was carried out as described previously (19). The NMR buffer (10 mM Tris, pH 7.0, 50 mM NaCl, 10% D$_2$0) was used for all assignment experiments. MqsA-C was concentrated to 0.5 mM. All experiments were performed at 293 K on a Bruker AvanceII 500-MHz spectrometer equipped with a TCI HCN *z*-gradient cryoprobe. The sequence-specific backbone assignment was obtained using the following experiments: two-dimensional ^{1}H,^{15}N HSQC, two-dimensional ^{1}H,^{13}C HSQC, three-dimensional HNCA, three-dimensional HNCACB, three-dimensional CBCA(CO)NH, three-dimensional (H)CC(CO)NH, and a three-dimensional HNCO spectrum. The NMR spectra were processed with Topspin 1.3 or 2.1 (Bruker, Billerica, MA) and analyzed using the CARA software package (available from the Swiss NMR Web site).

Assignments were obtained for more than 94% of all backbone nuclei (^{13}Cα, ^{13}Cβ, ^{13}CO, ^{15}N, and H$_N$). Of the 69 expected backbone amide N-H pairs (4 prolines), 65 were identified; missing ones correspond to two N-terminal cloning artifacts as well as residues Asn[97] and Ser[112] (supplemental Fig. S2). All chemical shifts were deposited in the BioMagResBank (available on the World Wide Web). An assignment of full-length MqsA is also available (52).

For all DNA interaction measurements, MqsA-C was exchanged into the NMR DNA buffer (10 mM Tris, pH 7.2, 50 mM NaCl, 1 mM EDTA). Complementary DNA oligonucleotides were also solubilized in NMR DNA buffer and annealed in equimolar concentrations. NMR titration experiments were performed by mixing ^{15}N-MqsA-C and each P*mqsRA* construct in a 1:1 ratio (100 μM each) and the addition of 10% (v/v) D$_2$O. Two-dimensional ^{1}H,^{15}N HSQC spectra (1024 × 128 real points) were recorded to analyze the interaction. Apo-MqsA-C spectra can be readily recorded (four scans). However, due to the high molecular mass of the MqsA-C·DNA complexes (~32 kDa), either 128 or 256 scans (7.5- or 15-h recording time, respectively) were necessary for a high quality two-dimensional ^{1}H,^{15}N HSQC spectrum.

Electrophoretic Mobility Shift Assay—Complementary oligonucleotides labeled with biotin at the 3′ end corresponding to the P*mqsRA* DNA used in crystallization studies were purchased (Integrated DNA Technologies), solubilized, and annealed as described previously (44). Also, complementary oligonucleotides corresponding to biotin-labeled P*mqsRA*-I were purchased and annealed. To determine dissociation constants, labeled WT P*mqsRA* DNA was incubated with a 10, 20, 40, 70, 100, 150, 200, 400, or 600 nM concentration of either wild type MqsA-F, MqsA-F N97A, MqsA-F R101A, or MqsA-F N97A/R101A (all proteins were purified immediately prior to EMSA experiments). A similar experiment using 50, 100, 150, 200, 250, 300, 350, 400, and 500 nM MqsA-C was also performed. To determine whether MqsA recognizes the P*mqsRA* DNA via a direct or indirect readout mechanism, 100 fmol of labeled DNA was mixed with a 50-fold excess of MqsA-F and a 200-fold excess of either WT or mutant unlabeled DNA. The binding reactions were incubated at room temperature for 20 min. Samples were then loaded onto a 6% DNA retardation gel (Invitrogen) and subjected to electrophoresis at 4 °C for 75 min and 100 V in TBE (45 mM Tris, pH 8.3, 45 mM boric acid, 1 mM EDTA) buffer. The DNA was transferred to a nylon membrane at 390 mA for 45 min and subsequently UV-cross-linked at 302 nm. Chemiluminescence was performed with the LightShift chemiluminescent EMSA kit (Pierce), and the samples were detected with a CCD imager (Typhoon 9410 imager). Integrated band volumes were calculated using ImageQuant TL software, and dissociation constants were calculated using Sigmaplot 8.0. All experiments were performed in triplicate except for MqsA-C, which was done in duplicate.

RESULTS

Structure of the MqsA·PmqsRA Complex—The structure of full-length MqsA (MqsA-F; residues 1–131; MqsA is a dimer) bound to the 26-mer DNA fragment corresponding to the palindrome of the *mqsRA* promoter (referred to hereafter as MqsA·P*mqsRA*) was determined to 2.1 Å resolution by molecular replacement (Fig. 1, *A–D*, and supplemental Fig. S1) using two copies of the MqsA N-terminal domain (MqsA-N), two copies of the MqsA C-terminal domain (MqsA-C), and four copies of a short 5-mer DNA duplex as search models. The space group is P4$_1$, with one copy of the MqsA·P*mqsRA* complex per asymmetric unit. The final model contains 264 protein residues and 52 nucleotides (Table 1).

The structure of the MqsA·P*mqsRA* complex reveals that a single MqsA dimer binds one P*mqsRA* DNA duplex using a large, positively charged surface on the undersides of the MqsA-C domains (Fig. 1*B*; the MqsA-C domain mediates dimerization). The MqsA dimerization axis is approximately perpendicular to the helical axis of DNA and passes through the center of the operator (base pair T14-A14′). Because the dimerization axis possesses nearly perfect 2-fold symmetry, the protein interactions with the two DNA palindrome half-sites are symmetric. The DNA is further enclosed by the MqsA-N domains, which make direct interactions with the DNA phosphate backbone. The interface between the MqsA protein and P*mqsRA* DNA is extensive, burying a total of
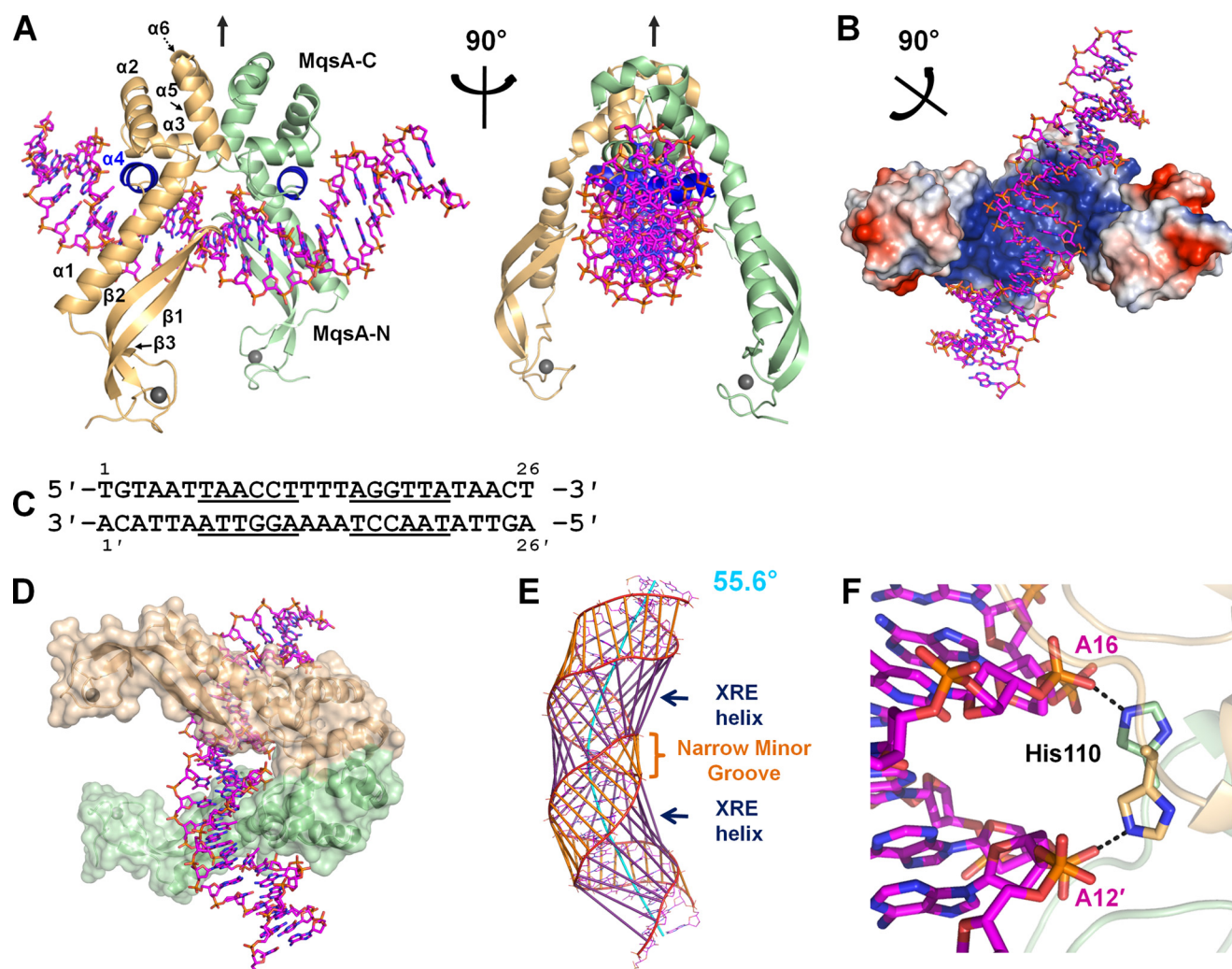
FIGURE 1. **The structure of the MqsA·P*mqsRA* transcriptional regulator complex.** *A*, the structure of MqsA·P*mqsRA* (*left* and *right panels* related by a 90° rotation about the pseudo-2-fold dimerization axis, which is indicated by a *black arrow*). The monomers of the MqsA dimer are *colored* in either *beige* or *green*, with the XRE recognition helix (α4) *colored* in *dark blue*; zinc ions are shown as *gray spheres*; and P*mqsRA* is shown as *sticks* and *colored* according to atom type. *B*, the MqsA·P*mqsRA* complex as shown from the underside of the dimer interface highlighting the DNA-binding surface. Shown is the electrostatic surface of MqsA (rotated by 90° as compared with the *middle panel*), with positive surface charge *colored blue*, negative surface charge in *red*, and neutral surface charge in *white*. There is a large positively charged surface patch along the DNA-binding pocket, which facilitates MqsA binding to the negatively charged dsDNA phosphate backbone. *C*, the sequence of the 26-mer dsDNA P*mqsRA* fragment bound by MqsA in the MqsA·P*mqsRA* crystal structure. The palindromic half-sites are *underlined*. *D*, MqsA·P*mqsRA* complex in which MqsA is represented as a solvent-accessible surface and the DNA is shown in *sticks* as in *A*. *E*, bound P*mqsRA* dsDNA represented as a *wire mesh* to illustrate the major (*purple lines*) and minor (*orange lines*) grooves. The DNA curves by 55.6°, and the axis of curvature is illustrated by a *light blue line* through the center of the DNA. This figure was generated using the program Curves+ (49). *F*, His[110] from each MqsA-C domain monomer (shown as *sticks*) is positioned to interact with the minor groove DNA backbone (*A12'* and *A16*) to help stabilize the DNA curvature. Polar interactions are indicated by a *black dashed line*.

3263 Å^2 of solvent-accessible surface area, ~13% of the solvent-accessible surface area of the entire complex.

MqsA Induces a Large Bend in the DNA—Complementarity between the DNA and MqsA is achieved by perturbations of the P*mqsRA* base pairs when compared with ideal B-form DNA. These perturbations result in an overall DNA curvature of 55.6°, enabling the MqsA-C recognition helices to bind symmetrically to each palindrome half-site (Fig. 1, *D* and *E*). Protein stabilization of bent DNA is often achieved by binding the minor groove at AT-rich sites (53). This mechanism of stabilization is also observed in the MqsA·P*mqsRA* complex. Namely, the P*mqsRA* palindrome half-sites are separated by a short AT-rich region (Fig. 1*C*). In the MqsA·P*mqsRA* complex, these nucleotides exhibit a collapsed minor groove and increased helical curvature when compared with ideal B-form

DNA. The collapsed minor groove is stabilized by multiple polar interactions between MqsA residues and the phosphate backbone. The central interaction, located at the most narrow region of the minor groove, is mediated by His[110] from each MqsA monomer. Specifically, both His[110] side chain NE2 atoms hydrogen bond with symmetrical phosphate oxygens from the opposing DNA strands (Fig. 1*F*). The narrowing of the minor groove is further stabilized by polar interactions from the MqsA-N domains, which serve to both "clamp" and immobilize the DNA.

DNA Sequence Recognition Is Mediated by the MqsA Recognition Helix Residues Asn[97] and Arg[101]—The MqsA·P*mqsRA* interface is composed of 40 protein residues (20 from each monomer) and 24 nucleotides (12 from each half-site) (Fig. 2*A*, protein-nucleotide interactions identified using Entangle)

TABLE 1

Crystallographic data collection and refinement statistics

	MqsA·P*mqsRA*
Data collection	
Space group	P4₁
Unit cell (Å)	$a = b = 60.99$, $c = 148.60$
Wavelength (Å)	0.9788
Resolution (Å)[a]	50.0-2.1 (2.14-2.10)
R_{merge} (%)[b]	0.075 (0.515)
Mean I/σ	29.13 (2.39)
Completeness (%)	99.5 (93.5)
Redundancy	6.7 (3.5)
Refinement	
Resolution range (Å)	47.15–2.10
R_{work} (%)	17.6
R_{free} (%)	22.76
Root mean square deviation	
Bond length (Å)	0.008
Bond angle (degrees)	1.163
Average B factor (Å²)	
Protein	27.9
Nucleic acid	38.8
Water	29.5
Ions	30.9
Ramachandran plot (%)	
Favored	97.7
Allowed	2.3
Disallowed	0

[a] Highest resolution shell data are shown in parentheses.
[b] $R_{merge} = \Sigma_{hkl}\Sigma_i|I_i(hkl) - \langle I(hkl)\rangle|/\Sigma_{hkl}\Sigma_i I_i(hkl)$ where $I_i(hkl)$ is the *i*th observation of a symmetry-equivalent reflection *hkl*.

(51). Thirty-two of the 40 protein residues responsible for binding the P*mqsRA* promoter are located in the MqsA-C domain, consistent with the MqsA-C domain being both necessary and sufficient to bind DNA (19). Previously, the MqsA-C domain was classified as a member of the XRE family of helix-turn-helix (XRE-HTH) proteins (19). Indeed, as predicted based on homology to other XRE-HTH proteins, the conserved XRE recognition helices (MqsA-C residues 97–104, *colored blue* in Fig. 1*A*) bind into the major groove of DNA. Both MqsA XRE recognition helices make equivalent interactions with each palindromic half-site.

Sequence recognition is mediated by residues Asn[97] and Arg[101] from the conserved XRE helix α4, which form discriminatory contacts with the DNA bases in the major groove (Fig. 2*B*). Asn[97] and Arg[101] make base-specific interactions with a total of eight nucleotides, four from one strand ([16]AGGT[19]) and four from the antiparallel strand ([18']CAAT[21']). In addition to hydrophobic and van der Waals interactions, Asn[97] and Arg[101] form key polar and hydrogen bonding interactions with the P*mqsRA* half-site nucleotide bases (Fig. 2*B*). Specifically, the side chain ND2 atom of Asn[97] forms hydrogen bonds with thymine 19 O4, whereas atom OD1 of Asn[97] forms a hydrogen bond with adenine 20′ N6. The guanidinium group nitrogens of Arg[101] also form polar contacts with guanine 17 N7 and guanine 18 O6. Additional base-specific interactions include hydrophobic contacts between the side chains of residues Val[96] and Ser[100] and the 5-methyl groups of thymine 19 and thymine 21′, respectively. These specific contacts are further stabilized by nonspecific interactions with the phosphate backbone. Additional nonspecific hydrogen bonds and salt bridge interactions from the MqsA-C domain are mediated by Arg[78] and Lys[79] in helix α2; Thr[84], Gln[85], and Lys[86] in helix α3; Gly[94] and Gly[95] in the

α3-α4 loop; Tyr[102] and Lys[104] in the conserved XRE helix α4; and Ala[107] and Gln[108] in the α4-α5 loop.

To elucidate the importance of Asn[97] and Arg[101] residues in DNA binding and transcription regulation, single mutants of both residues (MqsA-F N97A and MqsA-F R101A) as well as the double mutant (MqsA-F N97A/R101A) were generated and tested for their ability to bind and shift the 26-mer P*mqsRA* DNA fragment using EMSA (all experiments repeated in triplicate; size exclusion chromatography and circular dichroism polarimetry were used to verify that the mutations did not induce global changes in the protein structure prior to EMSA analysis; supplemental Fig. S3). In the presence of 20 nM WT MqsA-F (2-fold excess *versus* DNA), all of the labeled P*mqsRA* shifted, indicating complete binding (Fig. 2*C*). We also show that this shift is specific because the addition of excess unlabeled DNA abolished the shift of labeled DNA (supplemental Fig. S4). In contrast, at the same concentration, only a partial shift is observed for both single mutants, MqsA-F N97A and MqsA-F R101A, clearly indicating that they bind P*mqsRA* DNA less effectively than WT. The EMSA data were also used to quantify the interaction of the MqsA proteins (WT and mutants) with P*mqsRA* DNA. WT MqsA has the strongest affinity for P*mqsRA* DNA, with a K_d of 0.8 ± 0.4 nM. The interaction of P*mqsRA* with MqsA R101A is weaker, with a K_d of 7.5 ± 4.5 nM. Finally, as expected from our structural analysis, the interaction of P*mqsRA* with MqsA-F N97A is even weaker, with a K_d of only 40.1 ± 7.3 nM. Thus, these data clearly show that Asn[97] is much more important for DNA binding than Arg[101] because the MqsA-F R101A mutant binds DNA nearly 6-fold more strongly than the MqsA-F N97A mutant. Finally, the simultaneous mutation of both residues (double mutant MqsA-F N97A/R101A) completely abolished DNA binding (Fig. 2*C*), even at concentrations as high as 600 nM (60-fold excess). These data demonstrate that, as predicted by the MqsA·P*mqsRA* structure, both Asn[97] and Arg[101] are essential for DNA binding and sequence recognition.

In addition, it is very interesting to note that no N^H-N correlation peak in the two-dimensional ^{1}H,^{15}N HSQC spectrum of MqsA-C was detected for Asn[97] (supplemental Fig. S2). This indicates that Asn[97] must either undergo a μs-ms conformational exchange or exchange with the solvent without adopting a single major conformation in the unbound state. This might prime Asn[97] for its role in DNA binding because it will allow for a rapid, enthalpic adaptation of the DNA bound conformation. The only other unassigned MqsA residue, Ser[112], does not participate in DNA binding but rather is located in helix α5 at the MqsA-C dimer interface.

DNA Binding Is Accompanied by Extensive Domain Rearrangements in MqsA—In the absence of DNA, MqsA (PDB entry 3GN5) is a highly elongated dimer, composed of a central MqsA-C domain dimerization core, with the MqsA-N domains of each monomer projecting outward from the dimer core (Fig. 3*A*, *light blue*) (19). Upon binding DNA, the MqsA-C domain dimer stays essentially unchanged, superimposing with that from apo-MqsA with a root mean square deviation of 0.934 Å. The differences between the apo- and DNA-bound MqsA-C dimers are due to a small collapsing of
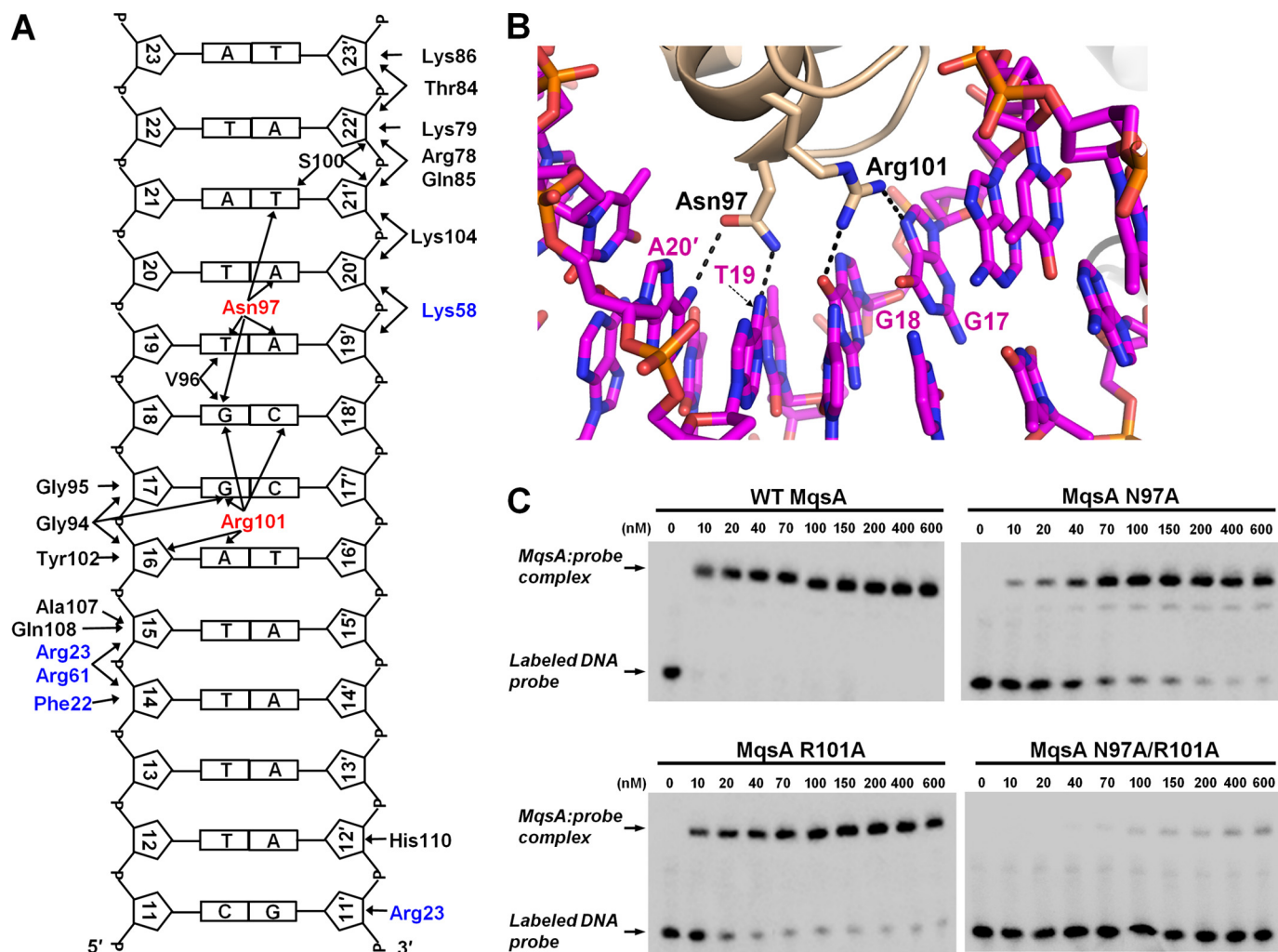
FIGURE 2. **MqsA specificity for P*mqsRA* is mediated by Asn[97] and Arg[101] and stabilized by multiple nonspecific interactions.** *A*, schematic diagram of all MqsA·P*mqsRA* interactions, including electrostatic, hydrogen bond, hydrophobic, and van der Waals interactions (identified using the program Entangle) (51). Interactions for only one palindrome half-site are shown because there are equivalent interactions with the second half-site. All residues that interact with DNA are labeled. The residues that mediate base-specific electrostatic contacts, Asn[97] and Arg[101], are labeled in *red*. Residues from the MqsA-N domain that stabilize DNA binding are labeled in *blue*. *B*, primary base-specific hydrogen bonding interactions (*dashed lines*) mediated by Asn[97] and Arg[101] (shown as *sticks*). Amino acid labels are shown in *black*, and nucleic acid labels are shown in *magenta*. *C*, EMSA experiments using biotin-labeled P*mqsRA* (the same construct used in crystallization) and increasing amounts of either WT MqsA, the MqsA single mutants (MqsA-F N97A or MqsA-F R101A), or the MqsA double mutant (MqsA-F N97A/R101A). WT MqsA (*top left*), MqsA-F N97A (*top right*), and MqsA-F R101A (*bottom left*) bind the P*mqsRA* construct as shown by a change in DNA migration as compared with the DNA alone (*lane 1* in each *panel*). However, the N97A and R101A mutants do so with a lower affinity than WT. MqsA-F N97A/R101A is unable to bind DNA (*bottom right*; gels have two control lanes that were removed for clarity, and full gels are shown in supplemental Fig. S6). All binding reactions contain the nonspecific poly(dI-dC) probe.

the XRE recognition helices toward the dimerization interface, which facilitates their interaction with DNA. This change is accommodated by the [93]GGG[95] loop that immediately precedes the XRE helices.

In contrast, both MqsA-N domains undergo extensive rearrangements upon binding DNA. Both MqsA-N domains rotate and twist by more than 106° (106°, monomer A; 120°, monomer B) (Fig. 3, *A* and *B*). This causes the MqsA-N domains to collapse about the DNA, transforming MqsA from a highly extended conformation into a narrow, elongated DNA "clamp." Unexpectedly, these rotations transform the MqsA dimerization axis from a pseudo- into a nearly perfect 2-fold axis between both monomers, allowing both MqsA-N domains to have symmetrical interactions with the bound DNA (Fig. 3*B*).

These domain rearrangements are mediated by a short, two-residue flexible segment linking the MqsA-N and MqsA-C domains, composed of residues Thr[68] and Val[69]. Flexibility between these domains has been shown previously by proteolytic digestion experiments (19). Whereas the MqsA-N and MqsA-C domains behave as rigid bodies, the Φ/Ψ angles of the residues in the linker undergo large changes, by ~45 and 165°, respectively, for Thr[68]. These DNA binding-induced rotations result in the formation of a novel interface between the MqsA-N and MqsA-C domains, which buries 627 Å² of solvent-accessible surface area (supplemental Fig. S5). The central residue of this new interface is MqsA-N residue Asn[65]. In the apo-MqsA structure, Asn[65] is entirely accessible to solvent. In contrast, in the DNA-bound structure, Asn[65], whose position changes by 7.8 Å as a conse-
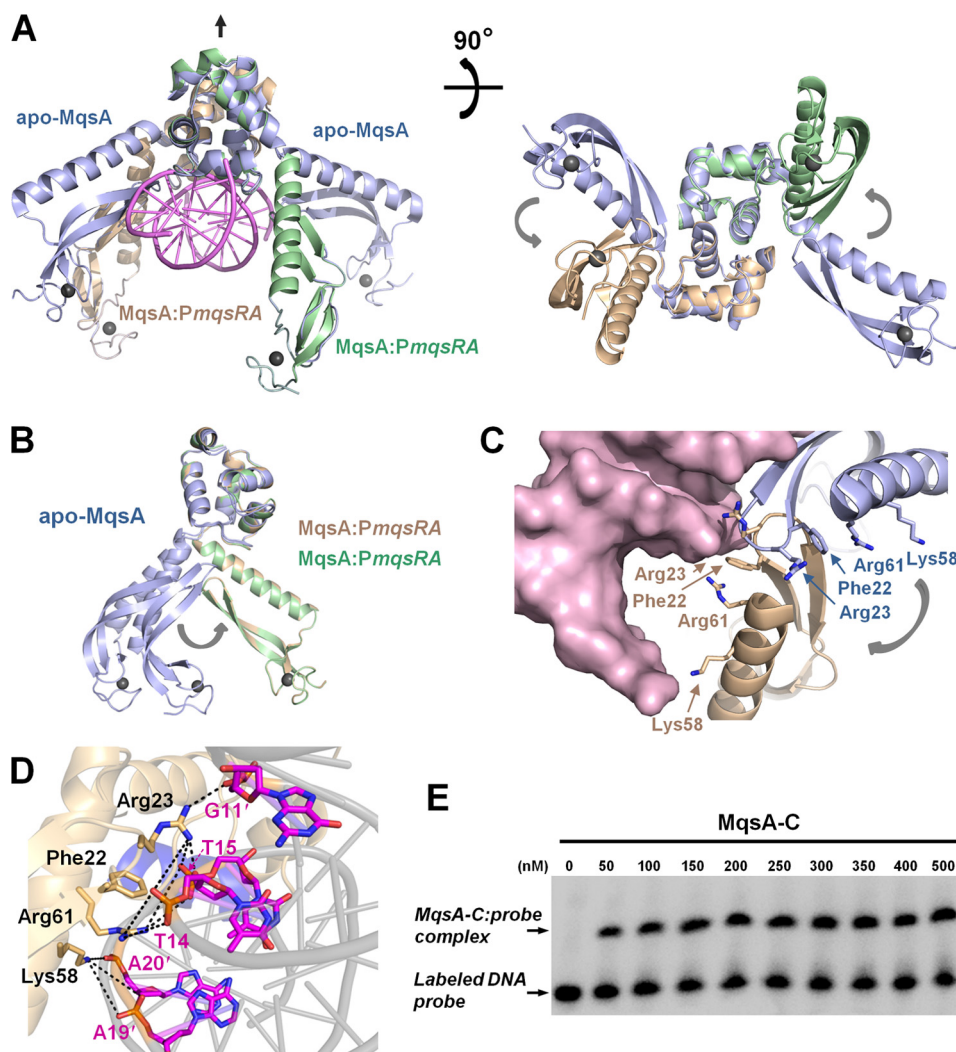
FIGURE 3. **The MqsA-N domains twist and rotate more than 105° upon binding DNA, forming a DNA "clamp."** *A*, apo-MqsA (*light blue*) with MqsA·PmqsRA (*colored* as in Fig. 1) superimposed on one another via the MqsA-C domain dimer illustrates the rotation and twist of each MqsA-N domain that occurs upon binding DNA (DNA is shown in *magenta*). *Right panel*, rotated by 90° about the indicated axis. *B*, the apo-MqsA-C domains from each monomer (*light blue*) superimposed on the corresponding domains from the MqsA·PmqsRA complex (*green*, *beige*) further illustrates the 106° and 120° rotations of the corresponding MqsA-N domains (rotations indicated by the *gray arrow*). In addition, superposition of MqsA monomers A (*beige*) and B (*green*) from the DNA-bound structure reveals that the MqsA-N domains are in identical positions relative to the MqsA-C-terminal domains. This shows that DNA binding imposes nearly perfect 2-fold symmetry on the conformation of the MqsA dimer. This differs from the apo-MqsA structure (monomers in *light blue*), in which the N-terminal domains are rotated by 36.9° with respect to one another via the Thr[68]-Val[69] hinge. *C*, the rotation of the MqsA-N domains causes four residues, Phe[22], Arg[23], Lys[58], and Arg[61], to move from an outward orientation, in which they are pointed away from the MqsA-C dimerization domain, to an inward orientation, in which they are positioned immediately below the MqsA-C dimerization domain and thus able to interact with the bound DNA. The DNA is illustrated as a *magenta surface*. *D*, electrostatic interactions and hydrophobic contacts between the MqsA-N residues and the DNA phosphate backbone. Residues Phe[22], Arg[23], Lys[58], and Arg[61] (shown as *sticks* with *black labels*) interact with the phosphate backbone of nucleotides G11', T14, T15, A19', and A20' (labeled in *magenta*). Polar interactions are indicated by *black dashes*; interactions for only one MqsA-N monomer are shown. *E*, the MqsA-N domain enhances DNA binding. Increasing amounts of MqsA-C were incubated with labeled DNA and monitored for protein binding. Compare with the *upper left panel* in Fig. 2*C* (MqsA-F). All binding reactions contain the nonspecific poly(dI-dC) probe.

quence of the MqsA-N domain rotation, is almost completely buried from solvent. In this conformation, the Asn[65]-ND2 atom hydrogen-bonds to the backbone carbonyl of Gly[105] from MqsA-C, whereas the Asn[65]-OD1 atom forms a hydrogen bond with Gln[108]-NE2. A second consequence of the MqsA-N rotation is that both residues Arg[23] and Arg[61] move from a position in which they face outwards, away from the dimer interface, into a position in which they face inwards, toward the bottom of the MqsA-C dimer (Fig. 3*C*).

Residues from the MqsA-N Domain Enhance DNA Binding— The structure of the MqsA·PmqsRA complex reveals that residues from the MqsA-N domain also contribute to DNA bind-

ing. The large rearrangement of the MqsA-N domains that accompanies DNA binding (Fig. 3, *A* and *B*) results in the formation of a DNA-binding pocket, with the C-terminal domain dimer forming the top of the pocket and the N-terminal domain β1-β2 turn and helix α1 forming the sides of the pocket. This structural change optimally positions multiple MqsA-N domain residues (Phe[22], Arg[23], Lys[58], and Arg[61]) for interaction with the bound DNA (Fig. 3, *C* and *D*). The most extensive interaction is mediated by Arg[23], which is located near the edge of the collapsed minor groove and abuts both MqsA-C domains. The guanidinium side chain of Arg[23] spans the minor groove, binding the DNA backbone phosphate oxy-

gens from each chain both directly, via salt bridge interactions, and indirectly, via water-mediated hydrogen bonds. Additional electrostatic interactions with the DNA sugar and phosphate backbone are mediated by MqsA-N residues Lys[58] and Arg[61], whereas hydrophobic interactions are mediated by Phe[22].

To demonstrate that the MqsA-N domain plays a role in DNA binding, we performed titration EMSA experiments with the 26-mer PmqsRA promoter DNA and the MqsA-C domain (Fig. 3E). As can be seen, the MqsA-C domain alone binds DNA more weakly than MqsA-F (compare Fig. 2C (*upper left*) with Fig. 3E) because 40–50 nM protein (4–5-fold excess) results in only a partial shift for MqsA-C (Fig. 3E) but a complete shift for MqsA-F (Fig. 2C, *upper left*). The EMSA data were also used to determine the dissociation constant for MqsA-C and PmqsRA (K_d = 41.5 ± 4.3 nM), which shows that MqsA-C binds PmqsRA 50-fold more weakly than MqsA-F (K_d = 0.8 ± 0.4 nM). Thus, the EMSA data confirm that the conformational changes between apo-MqsA and DNA-bound MqsA are biologically relevant.

MqsA Recognition of DNA Is Mediated by Direct Versus Indirect Readout—DNA sequence recognition by DNA-binding proteins is often mediated by direct readout, in which discriminatory interactions are made between the protein and the DNA bases. However, in some recognition events, no direct contacts are made between the protein and bases. Instead, in these cases, DNA recognition is mediated by indirect readout, in which the proteins bind distinct conformations of distorted, or bent, DNA; these DNA distortions are often accommodated by AT-rich sequences (42, 43, 53). Many members of the XRE family of DNA-binding proteins, including MqsA, make direct contacts with the DNA bases in the major groove via the XRE recognition helix (27, 54). However, many XRE DNA-binding proteins, including MqsA, bind bent DNA, with the DNA distortions accommodated near AT-rich segments, and thus these proteins may also use indirect readout for sequence recognition (27). The PmqsRA palindrome is separated by a short AT-rich segment ([13]TTT[15]) that, in the MqsA·PmqsRA complex, mediates the 55.6° DNA bend via a very narrowed minor groove (Fig. 1, *C* and *E*).

In order to determine the importance of direct *versus* indirect readout in sequence recognition by MqsA, we performed EMSA experiments coupled with NMR spectroscopy titration studies between MqsA and various WT and mutant PmqsRA DNA duplexes (Fig. 4, *A–D*). The NMR studies were performed with only the C-terminal domain because it is both necessary and sufficient for DNA binding (19), and it provides all of the base-specific DNA interactions. Furthermore, the size of the MqsA-C·PmqsRA complex (~32 kDa) is reasonable for NMR measurements, whereas the size of the full-length complex (~45.9 kDa) would make measurements exceedingly more difficult. For these interaction studies, the sequence-specific backbone assignment of the MqsA-C domain has been determined (supplemental Fig. S2).

To investigate the importance of direct readout in sequence recognition, two DNA mutants were generated in which the nucleotides involved in base-specific protein recognition were either mutated to the opposite purine or pyrimidine nucleo-

tides (*e.g.* A to G or T to C; PmqsRA-D1) or to the typical paired base of the opposite purine or pyrimidine (*e.g.* A to C or T to G; PmqsRA-D2; Table 2). EMSA competition experiments were performed to determine how effectively unlabeled mutant DNA duplexes prohibit the binding of labeled WT DNA. Specifically, a 50-fold molar excess of MqsA was incubated with labeled WT PmqsRA in the presence of an excess of unlabeled DNA (either WT or mutant) for 20 min and subsequently analyzed by EMSA to detect binding. As expected, the excess unlabeled WT PmqsRA DNA effectively out-competed the binding of the labeled WT DNA to MqsA, causing the intensity of the shifted band to disappear completely (Fig. 4A, lane 3). However, the addition of excess unlabeled mutant PmqsRA-D1 or PmqsRA-D2 DNAs resulted in no decrease in the intensities of the shifted bands (Fig. 4A, compare *lane 3* with *lanes 4* and *5*), demonstrating that the two mutant DNA duplexes are not able to out-compete WT DNA for MqsA.

We then used NMR spectroscopy to determine how the changes in binding between WT and mutant DNAs are mediated at a molecular level. Specifically, two-dimensional ^{1}H,^{15}N HSQC spectra were measured of the MqsA-C domain dimer alone and titrated with either WT or mutant DNA. Chemical shift differences between the spectra show changes of the local environment. As expected, in the presence of WT PmqsRA, many significant changes in chemical shifts between apo- and DNA-bound MqsA-C are observed, indicative of binding (Fig. 4B). However, upon the addition of either PmqsRA-D1 (Fig. 4C) or PmqsRA-D2 (data not shown), additional significant differences in the chemical shifts are observed when directly compared with WT PmqsRA, demonstrating that the mutant DNAs behave very differently from WT.

To determine if DNA geometry or curvature plays a role in protein binding, the three nucleotides in the intervening AT-rich region were mutated to GC base pairs (*e.g.* A to G or T to C; PmqsRA-I; Table 2). EMSA competition experiments showed that DNA mutant PmqsRA-I behaves virtually identically to WT PmqsRA, with unlabeled PmqsRA-I out-competing labeled PmqsRA for MqsA-C binding nearly as effectively as unlabeled WT PmqsRA (Fig. 4A, compare *lanes 3* and *6*). The dissociation constant of PmqsRA-I for MqsA-F (2.8 ± 0.6 nM) is also nearly identical to that of PmqsRA for MqsA-F (0.8 ± 0.4 nM; supplemental Fig. S6F). This demonstrates that the identity of the nucleotides separating the palindrome half-sites is not important because the three intervening nucleotides can be changed without significantly affecting the binding affinity of MqsA for PmqsRA. Furthermore, the NMR titration experiments confirm the EMSA competition results. Namely, the chemical shift changes in the two-dimensional ^{1}H,^{15}N HSQC spectrum of MqsA-C titrated with PmqsRA-I were nearly identical to those observed with WT PmqsRA (Fig. 4D), demonstrating that MqsA-C binds PmqsRA and PmqsRA-I via identical interactions. These results, in conjunction with the MqsA Asn[97] and Arg[101] mutant EMSA studies (Fig. 2C), show that MqsA mediates DNA sequence recognition using direct readout.
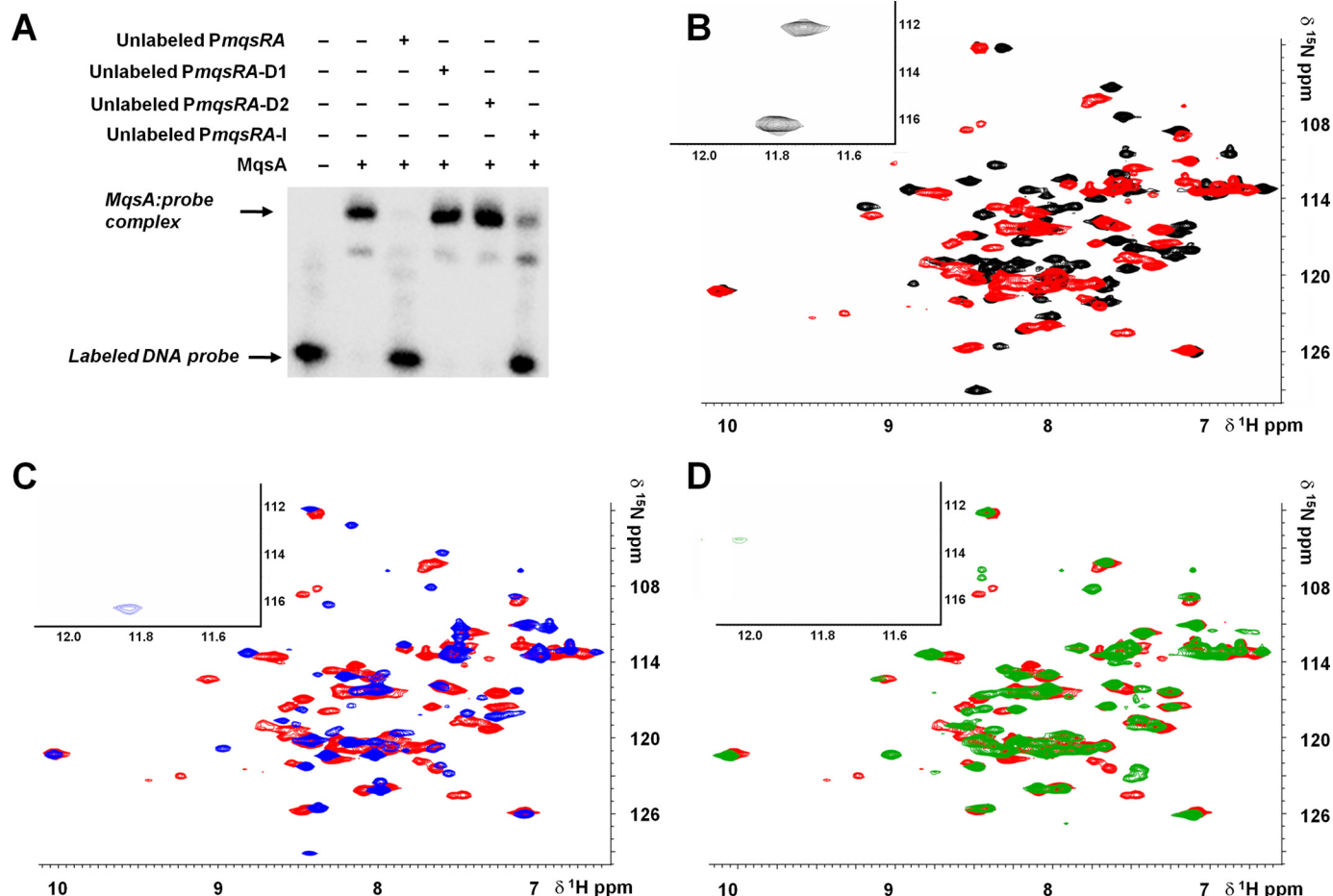
FIGURE 4. **MqsA recognition of its gene promoter is mediated by direct, and not indirect, readout.** *A*, EMSA experiments probing the importance of direct and indirect readout in MqsA-DNA recognition. The labeled DNA probe corresponds to the P*mqsRA* construct used in crystallization. Excess unlabeled DNA (WT or the mutant DNA constructs P*mqsRA*-D1, P*mqsRA*-D2, or P*mqsRA*-I) was used to compete with biotin-labeled WT DNA for binding MqsA. Unlabeled DNA constructs that bind MqsA show a decrease in the shifted MqsA·labeled DNA complex band. Both P*mqsRA*-D1 and P*mqsRA*-D2 constructs are unable to out-compete WT P*mqsRA* for MqsA binding (*lanes 4* and *5*, respectively), as shown by similarity to the control without excess unlabeled DNA (*lane 2*). However, P*mqsRA*-I binds MqsA nearly as effectively as WT P*mqsRA* (*lane 6*). These data demonstrate that MqsA utilizes a direct readout mechanism for sequence recognition. *B*, two-dimensional ^{1}H,^{15}N HSQC spectrum for the ^{15}N-labeled MqsA-C domain alone (*black*) overlaid with that of ^{15}N-labeled MqsA-C titrated with WT P*mqsRA* DNA (1:1 molar ratio; *red*). As can be seen, many peaks show significant changes of their chemical shifts upon titration with DNA, indicative of binding. *C*, two-dimensional ^{1}H,^{15}N HSQC spectrum for the ^{15}N-labeled MqsA-C domain titrated with WT P*mqsRA* (*red*) overlaid with that of the ^{15}N-labeled MqsA-C domain titrated with P*mqsRA*-D1 (*blue*). As can be seen, multiple peaks show changes of their chemical shifts indicating that P*mqsRA*-D1 does not behave like WT P*mqsRA* DNA. *D*, two-dimensional ^{1}H,^{15}N HSQC spectrum for the ^{15}N-labeled MqsA-C domain titrated with WT P*mqsRA* (*red*) overlaid with that of ^{15}N-labeled MqsA-C domain titrated with P*mqsRA*-I (*green*). As can be seen, the two spectra overlap extremely well, indicating that P*mqsRA*-I behaves nearly identically to WT P*mqsRA*.

TABLE 2

dsDNA mutant constructs used in NMR and EMSA experiments

Palindrome half-sites are underlined. Mutated bases are indicated with boldface type.

Name	Sequence (5′ → 3′)
WT P*mqsRA*	TGTAAT<u>TAACCTTTTAGGTTA</u>TAACT
P*mqsRA*-D1	TGTAAT<u>TA**GTT**TTTA**AAC**TA</u>TAACT
P*mqsRA*-D2	TGTAAT<u>TA**CAA**TTTA**TTG**TA</u>TAACT
P*mqsRA*-I	TGTAAT<u>TAACCT**CCC**AGGTTA</u>TAACT

DISCUSSION

DNA Binding by MqsA Is Unique among All Known Bacterial Antitoxins—These studies provide new and additional evidence that MqsA defines a novel family of antitoxins. First, MqsA binds DNA predominantly via its MqsA-C and not MqsA-N domains (Fig. 1), with 32 of the 40 residues contributing to DNA binding coming from the MqsA-C domain. Although MqsA binds bent DNA, whose collapsed minor groove is stabilized by multiple protein interactions, we showed that sequence recognition is mediated exclusively by direct readout (Fig. 4). XRE recognition helix residues Asn[97] and Arg[101] mediate the direct readout, making base-specific contacts with eight nucleotides from each palindrome half-site (Fig. 2). Moreover, when both residues are deleted, DNA binding is totally abolished. Several other MqsA-C residues also stabilize DNA binding through nonspecific interactions with the phosphate backbone or ribose sugar moieties. Second, in the presence of DNA, the MqsA-N domains twist and collapse by over 105° via a two-residue hinge that allows these domains to rotate freely as rigid bodies (Fig. 3). This rotation "clamps" the bound DNA and confers nearly perfect 2-fold symmetry of the MqsA dimer, previously unseen in the apo-MqsA structure. It also results in significant interactions between MqsA-N residues Phe[22], Arg[23], Lys[58], and Arg[61] with the DNA backbone. Indeed, the DNA binding affinity for full-
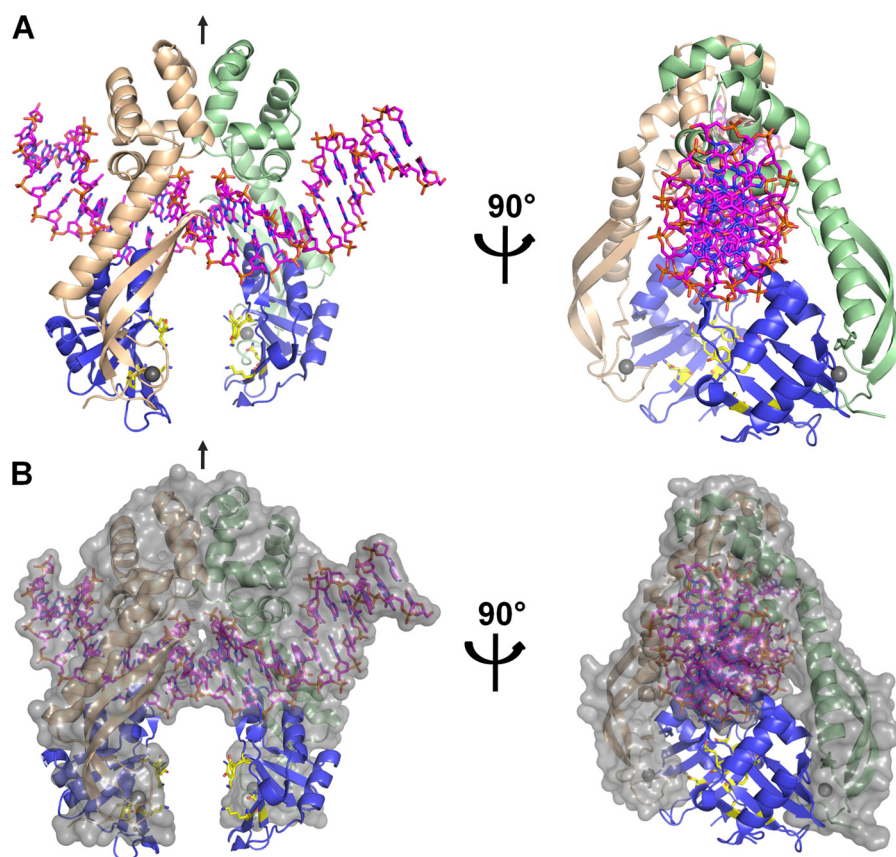
FIGURE 5. **Model of the MqsR·MqsA·P*mqsRA* transcriptional regulator complex.** A model of MqsR·MqsA·P*mqsRA* was generated by superimposing the previously solved MqsR·MqsA-N structure onto each N-terminal domain of the MqsA·P*mqsRA* structure. *A, left panel* shows MqsA·P*mqsRA* (*colored* as in Fig. 1) with one MqsR monomer (*blue*) bound to each N-terminal domain. MqsR functional site residues Lys[56], Gln[68], Tyr[81], and Lys[96] are shown as *sticks colored* in *yellow*. The 2-fold dimer interface is denoted with a *black arrow*. The *right panel* is rotated 90° about the indicated axis. Rotation of the MqsA N-terminal domains upon DNA binding brings the MqsR toxin molecules in close proximity to the DNA, suggestive of a direct interaction between MqsR and the DNA. *B*, same orientation as in *A* with the MqsA·P*mqsRA* structure shown as a surface representation (*gray*).

length MqsA is significantly higher than the binding affinity to the MqsA-C domain alone, further supporting the structural evidence that MqsA-N domains stabilize DNA binding (Fig. 3*E*). These domain rearrangements are unprecedented for DNA binding by a bacterial antitoxin.

To date, three antitoxin·DNA structures have been reported: the chromosome-encoded *hipBA* module from *E. coli* (27), the plasmid-encoded *ccdAB* module from *E. coli* (55), and the chromosome-encoded *fitAB* module from *Neisseria gonorrhoeae* (56). HipB, like MqsA, is one of the few antitoxins identified to date that recognizes DNA via an XRE-HTH DNA-binding motif (19, 27, 57, 58). Despite sharing a common DNA recognition fold, the sequence identity between the MqsA and HipB DNA-binding domains is only 16%.

As expected, both MqsA and HipB bind the major groove of DNA via their respective XRE recognition helices. However, because the MqsA and HipB dimerization interfaces are completely distinct from one another (supplemental Fig. S7), their bound DNAs curve in different directions. As a consequence, the XRE residues that mediate sequence recognition are also not conserved, either in position or in sequence (supplemental Fig. S7). Moreover, HipB binds both DNA and the HipA antitoxin via its structured N-terminal domain. Whether or not conformational changes accompany DNA binding remains to be determined because the apo-structure

of HipB has not yet been reported. However, because the HipB protein is composed nearly entirely of the XRE-HTH domain, large conformational changes like those observed in MqsA are not expected upon DNA binding.

In contrast, both the antitoxins CcdA and FitA recognize their operon promoters via a ribbon-helix-helix DNA-binding motif, in which the β-strands of the ribbon-helix-helix domain insert into the DNA major groove. In these proteins, the CcdA and FitA C-terminal toxin-binding domains do not interact with the bound DNA, and instead their DNA-binding and toxin-binding domains are entirely distinct. This differs significantly from MqsA, in which both the MqsA-C DNA-binding and the MqsA-N toxin-binding domains interact directly with the bound DNA. Aside from MqsA, whose structure is reported herein, the only antitoxin whose structure has been determined in both its apo- and DNA-bound state is CcdA (the structures of FitA and HipB have only been determined in the DNA-bound or toxin-bound state). In both the apo- and DNA-bound states, the CcdA toxin-binding domains are unstructured and do not contribute to DNA binding. In contrast, the MqsA-N domain, which binds the MqsR toxin, makes direct interactions with DNA and enhances DNA binding even in the absence of MqsR. Only MqsA, which is unique among antitoxins because it is structured throughout its entire sequence in both the apo-, DNA-bound,

and toxin-bound forms, exhibits the extensive conformational changes of the MqsA-N domains between the apo- and DNA-bound states that stabilize the MqsA·P*mqsRA* complex and enhance DNA binding (Fig. 3).

MqsR·MqsA·PmqsRA Model Predicts a Role for the MqsR Toxin in Transcriptional Co-regulation—Neither MqsR (35) nor the MqsR·MqsA-N complex (19) is capable of binding DNA. However, it is well established across many TA systems, including MqsR·MqsA (35), that TA complexes bind the operon promoter with higher affinity than the antitoxin alone. Two toxin·antitoxin·DNA structures are currently available (FitB·FitA·DNA (56) and HipA·HipB·DNA (27)), and each displays a different mechanism of toxin co-regulation. In the case of the FitAB module, two FitB toxin monomers bind to two FitA antitoxin dimers to form a heterotetramer. This serves to "tether" the FitA antitoxin dimers on the DNA. Although the toxins do not interact with DNA, they facilitate binding by stabilizing the FitAB heterotetramer. In contrast, in the case of the HipBA module from *E. coli*, the HipA toxin interacts directly with the DNA backbone. In this case, DNA binding is enhanced through direct interactions between the DNA and the toxin.

To determine the potential mechanism utilized by the *mqsRA* TA module, we generated a model of the MqsR·MqsA·P*mqsRA* transcriptional regulator complex by superimposing the structure of the MqsR·MqsA-N complex (19) with the MqsA·P*mqsRA* complex (Fig. 5). Our model of the MqsR·MqsA·P*mqsRA* complex shows that the large rearrangements of the MqsA-N domains that occur upon DNA binding position the bound toxins directly below the XRE recognition helices. This would enable the toxins to interact with the bound DNA, most likely via nonspecific interactions with the phosphate backbone because MqsR itself does not bind DNA (19, 35). Thus, this model predicts that the *mqsRA* TA module most likely utilizes a mechanism of transcriptional co-regulation in which the MqsR toxin interacts directly with the P*mqsRA* DNA, a mechanism similar to that seen with the *hip*BA TA module.

MqsR Toxicity Is Mitigated by Steric Occlusion—Our model also provides new insights into the mechanism used by MqsA to mitigate MqsR-mediated toxicity. Previously identified residues that comprise the MqsR active site are Lys[56], Gln[68], Tyr[81], and Lys[96], all of which are accessible when bound to the MqsA-N domain (19). Unexpectedly, in the MqsR·MqsA·P*mqsRA* complex model, these residues are now facing inward, toward the pseudo-2-fold rotation axis of the MqsA dimer and underneath the bound DNA (Fig. 5). In this DNA-bound orientation, the active sites of the two MqsR toxins face one another and are separated by only ~13–15 Å. This orientation probably severely limits the accessibility of the active sites for mRNA and/or the ribosome, supporting a mechanism of toxin neutralization through steric occlusion.

CONCLUSIONS

The structure of the MqsA·P*mqsRA* transcription-regulatory complex provides new evidence that MqsA is highly unique among all known antitoxins. Unlike other antitoxins,

MqsA requires metal for structural stability; toxin binding is mediated by the N-terminal domain, whereas DNA binding is mediated by the C-terminal HTH domain; and, most significantly, MqsA is structured throughout its entire sequence in the free, the toxin-bound, and now the DNA-bound forms (19). The structure of the MqsA·P*mqsRA* complex now reveals that MqsA is also unique because, unlike other antitoxins, MqsA undergoes unprecedented domain rearrangements upon binding DNA. These rotations result in orientations of the MqsA-N domains that enable the MqsR toxins to bind directly to the DNA, providing a molecular basis for the observation that MqsR enhances DNA binding and stability. Finally, these conformational changes provide new evidence that MqsA neutralizes MqsR toxicity by steric occlusion because, as modeled when bound to DNA, the MqsR functional sites face one another and define a narrow 13–15-Å channel immediately below the bound DNA, making them nearly inaccessible to other biomacromolecules, such as mRNA. Therefore, this work has provided the first insights into understanding how this unique antitoxin regulates transcription at a molecular level and provides a basis for developing novel antibacterial therapies that target TA pairs.

REFERENCES

1. Lopez, D., Vlamakis, H., and Kolter, R. (2010) *Cold Spring Harb. Perspect. Biol.* **2,** a000398
2. Cos, P., Tote, K., Horemans, T., and Maes, L. (2010) *Curr. Pharm. Des.* **16,** 2279–2295
3. Anderson, G. G., and O'Toole, G. A. (2008) *Curr. Top. Microbiol. Immunol.* **322,** 85–105
4. Keren, I., Shah, D., Spoering, A., Kaldalu, N., and Lewis, K. (2004) *J. Bacteriol.* **186,** 8172–8180
5. del Pozo, J. L., and Patel, R. (2007) *Clin. Pharmacol. Ther.* **82,** 204–209
6. Stewart, P. S. (2002) *Int. J. Med. Microbiol.* **292,** 107–113
7. Bigger, J. W. (1944) *Lancet* **244,** 497–500
8. Korch, S. B., Henderson, T. A., and Hill, T. M. (2003) *Mol. Microbiol.* **50,** 1199–1213
9. Black, D. S., Kelly, A. J., Mardis, M. J., and Moyed, H. S. (1991) *J. Bacteriol.* **173,** 5732–5739
10. Spoering, A. L., and Lewis, K. (2001) *J. Bacteriol.* **183,** 6746–6751
11. Vázquez-Laslop, N., Lee, H., and Neyfakh, A. A. (2006) *J. Bacteriol.* **188,** 3494–3497
12. Shah, D., Zhang, Z., Khodursky, A., Kaldalu, N., Kurg, K., and Lewis, K. (2006) *BMC Microbiol.* **6,** 53
13. Gerdes, K., Christensen, S. K., and Løbner-Olesen, A. (2005) *Nat. Rev. Microbiol.* **3,** 371–382
14. Gerdes, K., Rasmussen, P. B., and Molin, S. (1986) *Proc. Natl. Acad. Sci. U.S.A.* **83,** 3116–3120
15. Magnuson, R. D. (2007) *J. Bacteriol.* **189,** 6089–6092
16. Ogura, T., and Hiraga, S. (1983) *Proc. Natl. Acad. Sci. U.S.A.* **80,** 4784–4788
17. Sevin, E. W., and Barloy-Hubler, F. (2007) *Genome. Biol.* **8,** R155
18. Van Melderen, L., and Saavedra De Bast, M. (2009) *PLoS Genet.* **5,** e1000437
19. Brown, B. L., Grigoriu, S., Kim, Y., Arruda, J. M., Davenport, A., Wood,

T. K., Peti, W., and Page, R. (2009) *PLoS Pathog.* **5,** e1000706

20. Dalton, K. M., and Crosson, S. (2010) *Biochemistry* **49,** 2205–2215
21. Van Melderen, L., Bernard, P., and Couturier, M. (1994) *Mol. Microbiol.* **11,** 1151–1157
22. Christensen, S. K., Pedersen, K., Hansen, F. G., and Gerdes, K. (2003) *J. Mol. Biol.* **332,** 809–819
23. Hiraga, S., Jaffé, A., Ogura, T., Mori, H., and Takahashi, H. (1986) *J. Bacteriol.* **166,** 100–104
24. Lehnherr, H., and Yarmolinsky, M. B. (1995) *Proc. Natl. Acad. Sci. U.S.A.* **92,** 3274–3277
25. Jiang, Y., Pogliano, J., Helinski, D. R., and Konieczny, I. (2002) *Mol. Microbiol.* **44,** 971–979
26. Pedersen, K., Zavialov, A. V., Pavlov, M. Y., Elf, J., Gerdes, K., and Ehrenberg, M. (2003) *Cell* **112,** 131–140
27. Schumacher, M. A., Piro, K. M., Xu, W., Hansen, S., Lewis, K., and Brennan, R. G. (2009) *Science* **323,** 396–401
28. de Feyter, R., Wallace, C., and Lane, D. (1989) *Mol. Gen. Genet.* **218,** 481–486
29. Magnuson, R., and Yarmolinsky, M. B. (1998) *J. Bacteriol.* **180,** 6342–6351
30. Tam, J. E., and Kline, B. C. (1989) *Mol. Gen. Genet.* **219,** 26–32
31. Kim, Y., Wang, X., Zhang, X. S., Grigoriu, S., Page, R., Peti, W., and Wood, T. K. (2010) *Environ. Microbiol.* **12,** 1105–1121
32. Ren, D., Bedzyk, L. A., Thomas, S. M., Ye, R. W., and Wood, T. K. (2004) *Appl. Microbiol. Biotechnol.* **64,** 515–524
33. González Barrios, A. F., Zuo, R., Hashimoto, Y., Yang, L., Bentley, W. E., and Wood, T. K. (2006) *J. Bacteriol.* **188,** 305–316
34. Christensen-Dalsgaard, M., Jørgensen, M. G., and Gerdes, K. (2010) *Mol. Microbiol.* **75,** 333–348
35. Yamaguchi, Y., Park, J. H., and Inouye, M. (2009) *J. Biol. Chem.* **284,** 28746–28753
36. Kamada, K., and Hanaoka, F. (2005) *Mol. Cell.* **19,** 497–509
37. Kamada, K., Hanaoka, F., and Burley, S. K. (2003) *Mol. Cell.* **11,** 875–884
38. Kumar, P., Issac, B., Dodson, E. J., Turkenburg, J. P., and Mande, S. C. (2008) *J. Mol. Biol.* **383,** 482–493
39. Takagi, H., Kakuta, Y., Okada, T., Yao, M., Tanaka, I., and Kimura, M. (2005) *Nat. Struct. Mol. Biol.* **12,** 327–331
40. Kasari, V., Kurg, K., Margus, T., Tenson, T., and Kaldalu, N. (2010) *J. Bacteriol.* **192,** 2908–2919
41. Haran, T. E., and Mohanty, U. (2009) *Q. Rev. Biophys.* **42,** 41–81
42. Lawson, C. L., and Breman, H. M. (2008) *Indirect Readout of DNA Sequence by Proteins,* (Rice, P. A., and Correll, C. C., eds), pp. 66–90, The Royal Society of Chemistry, Cambridge
43. Little, E. J., Babic, A. C., and Horton, N. C. (2008) *Structure* **16,** 1828–1837
44. Brown, B. L., and Page, R. (2010) *Acta Crystallogr. F* **66,** 1060–1063
45. Otwinowski, Z., and Minor, W. (1997) *Macromol. Crystallogr. A* **276,** 307–326
46. Adams, P. D., Afonine, P. V., Bunkóczi, G., Chen, V. B., Davis, I. W., Echols, N., Headd, J. J., Hung, L. W., Kapral, G. J., Grosse-Kunstleve, R. W., McCoy, A. J., Moriarty, N. W., Oeffner, R., Read, R. J., Richardson, D. C., Richardson, J. S., Terwilliger, T. C., and Zwart, P. H. (2010) *Acta Crystallogr. D Biol. Crystallogr.* **66,** 213–221
47. McCoy, A. J., Grosse-Kunstleve, R. W., Adams, P. D., Winn, M. D., Storoni, L. C., and Read, R. J. (2007) *J. Appl Crystallogr.* **40,** 658–674
48. Emsley, P., and Cowtan, K. (2004) *Acta Crystallogr. D Biol. Crystallogr.* **60,** 2126–2132
49. Lavery, R., Moakher, M., Maddocks, J. H., Petkeviciute, D., and Zakrzewska, K. (2009) *Nucleic Acids Res.* **37,** 5917–5929
50. Lu, X. J., and Olson, W. K. (2008) *Nat. Protoc.* **3,** 1213–1227
51. Allers, J., and Shamoo, Y. (2001) *J. Mol. Biol.* **311,** 75–86
52. Papadopoulos, E., Billeter, M., Gräslund, A., and Vlamis-Gardikas, A. (2007) *Biomol. NMR Assign.* **1,** 217–219
53. Privalov, P. L., Dragan, A. I., and Crane-Robinson, C. (2009) *Trends Biochem. Sci.* **34,** 464–470
54. Watkins, D., Hsiao, C., Woods, K. K., Koudelka, G. B., and Williams, L. D. (2008) *Biochemistry* **47,** 2325–2338
55. Madl, T., Van Melderen, L., Mine, N., Respondek, M., Oberer, M., Keller, W., Khatai, L., and Zangger, K. (2006) *J. Mol. Biol.* **364,** 170–185
56. Mattison, K., Wilbur, J. S., So, M., and Brennan, R. G. (2006) *J. Biol. Chem.* **281,** 37942–37951
57. Arbing, M. A., Handelman, S. K., Kuzin, A. P., Verdon, G., Wang, C., Su, M., Rothenbacher, F. P., Abashidze, M., Liu, M., Hurley, J. M., Xiao, R., Acton, T., Inouye, M., Montelione, G. T., Woychik, N. A., and Hunt, J. F. (2010) *Structure* **18,** 996–1010
58. Button, J. E., Silhavy, T. J., and Ruiz, N. (2007) *J. Bacteriol.* **189,** 1523–1530